Validity of analytical formulas for autoionization and dielectronic capture rates used in collisional-radiative models

Cheng Gao and Jiaolong Zeng*

Department of Physics, College of Science, National University of Defense Technology, Changsha Hunan, P.R. China, 410073

(Received 25 September 2010; published 22 December 2010)

Large-scale level-by-level calculations were carried out to obtain as accurate autoionization and dielectronic capture (DC) rates of Ni-like Au^{51+} and Cu-like Au^{50+} as possible by including adequate electron correlations. The accuracy is estimated to be better than 20% for strong autoionized levels. Our results of the dielectronic recombination (DR) process through $3d^9 4lnl'$ ($n = 4,5$) agree excellently (within 10%) with other theoretical results also obtained by detailed level-by-level calculations reported in the literature. The level-by-level results were transformed to configuration-by-configuration autoionization and DC rates (which are estimated to be better than 30% in accuracy) and used to check the validity of the rate coefficients in collisonal-radiative (CR) models by using an analytical formula. Large discrepancies were found between the detailed calculated rates and those predicted by the analytical formula. The autoionization and DC rates predicted by the analytical formula can be more than two orders of magnitude larger than the detailed calculated rates, in particular for the autoionized configurations whose energy is near the ionization potential (IP). However, for those autoionized configurations whose energy is far above the IP, the autoionization and DC rates predicted by the analytical formula can be nearly one order of magnitude smaller. Differences between different theoretical methods found in this work, when approximate methods are used to calculate the autoionization and DC rates, would result in differences when non–local-thermodynamic-equilibrium (NLTE) models used the less accurate methods to obtain these atomic data.

DOI: 10.1103/PhysRevA.82.062515 PACS number(s): 31.15.am, 32.80.Zb

I. INTRODUCTION

Population kinetics and radiative properties of high-temperature non–local-thermodynamic-equilibrium (NLTE) plasmas are of great interest since they have important applications in the research of inertial confinement fusion (ICF), x-ray lasers, astrophysics, and extreme ultraviolet (EUV) lithography. A great effort has been devoted to this research field and a series of progress has been achieved. Much of this progress is the result of a series of NLTE workshops dedicated to comparing the results from different codes and computational approaches applied to a series of test problems [1–5]. These workshops are very useful in determining in which regimes a high degree of confidence may be had in the quality of the plasma model. Recently, Chung and Lee [6] gave a review of applications of NLTE population kinetics for a number of elaborately selected research fields. Scott and Hansen [7] reported advances in NLTE modeling for integrated simulations using a simple screened-hydrogenic model which can be used as a routine in radiation-hydrodynamics codes.

Autoionization and dielectronic capture (DC) play an important role in these NLTE modelings. The NLTE code comparison workshops and many other research [8–15] highlighted the importance of the autoionization and DC processes to determine the population balance and radiative properties in plasmas with a wide range of temperature and density. From the comparisons of different codes in NLTE workshops one can conclude that a much better agreement is found for different codes without the inclusion of the autoionization and electron capture processes in the collisional-radiative (CR) model. However, a much better agreement can be obtained between the theoretical results with the autoionization and DC processes being taken into account and the experiments. Why is there such a dramatic discrepancy for different models when the autoionization and DC processes are taken into account? The first thing one should do is to check the accuracy of the rate coefficients contributed by the autoionization and DC processes used in different codes. To solve the discrepancy, one possible direction should be toward improving the accuracy of the relevant rate coefficients.

However, such an endeavor is difficult due to the complexity of the atomic model that underlies the CR model. In principle, the most detailed level of information is referred to as the detailed level accounting (DLA) model, where each atomic level is explicitly included and the solution of a level-by-level kinetic model is required. Yet this approach is considered practical for low and medium atomic numbers ($Z < 30$) [16–19]. As the atomic number increases, the DLA approach becomes impractical and a detailed configuration accounting (DCA) model is the usual choice. To obtain accurate rate coefficients of the autoionization and DC processes, one should choose accurate theoretical methods based on atomic structure and scattering calculations. However, due to the complexity of this problem, a number of codes employed analytical expressions based on different approximations or some kinds of statistical methods [6,20,21].

In this work, we checked the accuracy of the autoionization and DC rates used in various DCA models by carrying out large-scale configuration interaction (CI) calculations, taking the DC process of Ni-like Au^{51+} and autoionization process of Cu-like Au^{50+} as an example. The configuration-by-configuration rate coefficients were obtained from the detailed level-by-level results.

*jiaolongzeng@hotmail.com

II. THEORETICAL METHOD

The detailed level-by-level calculations were carried out using a distorted-wave approximation implemented by the Flexible Atomic Code (FAC) developed by Gu [22]. A fully relativistic approach based on the Dirac equation is used throughout the entire package. An atomic state is approximated by a linear combination of configuration state functions (CSF's) with the same symmetry

$$\Phi_\alpha(J\pi) = \sum_i^{n_c} a_i(\alpha)\phi_\alpha(J\pi), \tag{1}$$

where n_c is the number of CSF's and $a_i(\alpha)$ denotes the representation of the atomic state in this basis. The CSF's are antisymmetrized products of a common set of orthogonal orbitals which are optimized on the basis of the relativistic Hamiltonian. The radial orbitals are derived from a modified Dirac-Fock-Slater iteration on a fictitious mean configuration with fractional occupation numbers, representing the average electron cloud of the configurations included in the calculation.

The autoionization and DC rates are obtained in the relativistic distorted-wave approximation. In the first-order perturbation theory, the autoionization rate can be written as (in atomic units)

$$A^a_{ij} = \sum_\kappa \left| \langle \psi_j, \kappa; J_T M_T | \sum_{i<j} \frac{1}{r_{ij}} | \psi_i \rangle \right|^2, \tag{2}$$

where ψ_i is the autoioning state, ψ_j is the final state which has one less electron than ψ_i, and κ is the relativistic angular quantum number of the free electron. The total angular quantum number of the coupled final state must be equal to that of ψ_i (i.e., $J_T = J_i$ and $M_T = M_i$). The DC rates can be evaluated by the principle of detailed balance. Assuming a Maxwellian electron velocity distribution corresponding to an electron temperature T_e, one obtains the electron capture rate coefficient [23]

$$\beta_{ji} = \frac{h^3}{2(2\pi m_e k T_e)^{3/2}} \frac{g_i}{g_j} A^a_{ij} e^{-E_{ij}/kT_e}, \tag{3}$$

where $E_{ij} = E_i - E_j$, g_i and g_j are the statistical weights of the respective levels. To obtain accurate atomic data, one should include adequate CI effects in both autoionized and recombined ions.

III. RESULTS AND DISCUSSION

Large-scale CI calculations were carried out to obtain the autoionization rate of Au^{50+}. In the present work, the fine-structure levels belonging to the following configurations of Au^{50+} are explicitly considered: $([1s^2 2s^2 2p^6])3s^2 3p^6 3d^{10} nl$, $3s^2 3p^6 3d^9 4lnl'$ $(n = 4,5,6,\ldots,9)$, $3s^2 3p^5 3d^{10} 4lnl'$, $3s3p^6 3d^{10} 4lnl'$ $(n = 4,5, l = 0,1,2,3,\ l' = 0,1,2,\ldots,n-1)$, and the configurations of Au^{51+} are $3s^2 3p^6 3d^{10}$, $3s^2 3p^6 3d^9 nl$, $3s^2 3p^5 3d^{10} nl$, $3s3p^6 3d^{10} nl$, $(n = 4,5,6,\ldots,9,$ $l = 1,2,3,\ldots,n-1)$; $3s^2 3p^6 3d^8 4l4l'$, $3s^2 3p^5 3d^9 4l4l'$, $3s^2 3p^4 3d^{10} 4l4l'$ $(l,l' = 0,1,2,3)$.

There are so many autoionized levels of Au^{50+} that it is not necessary to give all of them here. As illustrative examples, Table I shows autoionization rates of Au^{50+} from energy levels belonging to the doubly excited configurations $3d^9 4l4l'$ and $3d^9 4l5l'$ to the ground level of Au^{51+}. To limit the data set, we only give the autoionization rates which are larger than 5.0×10^{13} s^{-1}. The autoionization rate is sensitive to the electron correlations included in the calculation. For the given rates, CI is adequately included to obtain the converged results. To show this convergence, two additional cases of calculations A and B with smaller scale CI were carried out and the results were given in Table I. In case A, configurations of $3s^2 3p^6 3d^{10} nl$ and $3s^2 3p^6 3d^9 4lnl'$ $(n = 4,5, l = 0,1,2,3, l' = 0,1,2,\ldots,n-1)$ of Au^{50+} and $3s^2 3p^6 3d^{10}$, $3s^2 3p^6 3d^9 nl$ and $3s^2 3p^6 3d^8 4l4l'$ $(n = 4,5,\ l,l' = 1,2,3,\ldots,n-1)$ of Au^{51+} were included in the calculation. In case B, further configurations of $3s^2 3p^5 3d^{10} 4lnl'$ and $3s3p^6 3d^{10} 4lnl'$ $(n = 4,5,$ $l = 0,1,2,3, l' = 0,1,2,\ldots,n-1)$ than case A were added for Au^{50+} and $3s^2 3p^5 3d^{10} nl$, $3s3p^6 3d^{10} nl$ and $3s^2 3p^5 3d^9 4l4l'$ $(n$=4, 5, l=0, 1, 2, 3, $l' = 0,1,2,\ldots,n-1)$ were added for Au^{51+}. In Table I, the results obtained by the previous large-scale CI are denoted as case C. The convergence trend can easily be seen from cases A to B and then to C. Most of the autoionization rates obtained by cases B and C agree with each other within 5% or even better. Therefore, the results of case C have converged. The autoionization rate is, in general, larger than the dipole radiative transition rate by one to two orders of magnitude, and therefore the autoionization and DC processes will dominate the population kinetics in some cases. However, accurate rate coefficients for these two processes are important for any CR modeling of population kinetics.

The DC process can be followed by radiative decay which is called dielectronic recombination (DR) and it is an important physical parameter for the coronal equilibrium plasmas [24–26]. Behar *et al.* [27] calculated the DR rate coefficients of ten ions along the Ni I isoelectronic sequence in the ground state of Au^{51+} through the Cu-like $3d^9 4ln'l'$ $(n' = 4,5)$ configurations using the HULLAC code package. The DR rate coefficient of the level i of the recombined ion reads as

$$\alpha(i) = \sum_j \beta_{ij} B_j, \tag{4}$$

where j is an autoionization level of autoionized ion and β_{ij} is the DC rate coefficient expressed in Eq. (3). The radiative stabilizing branching ratio B_j reads as

$$B_j = \frac{\sum_k A^r_{jk} + \sum_{k'} A^r_{jk'} B_{k'}}{\sum_m A^a_{jm} + \sum_s A^r_{js}}, \tag{5}$$

where $\sum_m A^a_{jm}$ is the total autoionization rate from the level of j and A^r_{js} is the radiative transition rate from level j to s, and k and k' represent the final levels with the energy of k being below the IP and k' above the IP. Level k' may further autoionize with an associated radiative stabilizing branching ratio $B_{k'}$.

Figure 1 compares our calculated DR rate coefficients of Au^{51+} in the ground state in a solid line through Fig. 1(a) $3d^9 4l4l'$ and (b) $3d^9 4l5l'$ of Au^{50+}, respectively, with those of Behar *et al.* [27] (circles) and Shi *et al.* [24] (squares). Shi *et al.* [24] used the FAC code [22] to obtain their results, thus using the same method as our work. It can easily be seen that different theoretical results agree well with each

TABLE I. Autoionization rates from the levels belonging to configurations $3d^9 4l 4l'$ and $3d^9 4l 5l'$ to the ground state of Ni-like Au^{51+}, where only the rates larger than 5.0×10^{13} (s^{-1}) are listed. $X[Y]$ denotes $X \times 10^Y$, J is the total angular momentum, and ΔE is the energy difference above the ionization limit. See details in the text for the description of cases A, B, and C.

			A^a (s^{-1})		
Conf.	J	ΔE (eV)	A	B	C
$(3d_{5/2}^{-1}4d_{5/2})_0 4f_{5/2}$	5/2	8.81	2.5584(14)	2.6661(14)	2.6756(14)
$(3d_{5/2}^{-1}4d_{5/2})_0 4f_{7/2}$	7/2	15.18	2.1945(14)	2.1706(14)	2.1439(14)
$(3d_{5/2}^{-1}4d_{5/2})_5 4f_{7/2}$	3/2	15.34	6.1562(13)	6.1107(13)	6.2594(13)
$(3d_{3/2}^{-1}4d_{3/2})_3 4f_{5/2}$	5/2	52.82	8.5028(13)	9.1582(13)	9.1124(13)
$(3d_{3/2}^{-1}4d_{3/2})_2 4f_{5/2}$	5/2	65.33	2.8315(14)	2.7641(14)	2.6677(14)
$(3d_{3/2}^{-1}4d_{5/2})_1 4f_{5/2}$	5/2	67.47	5.5259(13)	6.7082(13)	7.2496(13)
$(3d_{3/2}^{-1}4d_{3/2})_3 4f_{5/2}$	1/2	70.82	5.5926(13)	6.3952(13)	6.3355(13)
$(3d_{3/2}^{-1}4d_{3/2})_0 4f_{5/2}$	5/2	88.40	3.4242(14)	2.3500(14)	2.3406(14)
$(3d_{3/2}^{-1}4d_{5/2})_4 4f_{5/2}$	3/2	102.72	1.0117(14)	1.0113(14)	1.0602(14)
$(3d_{3/2}^{-1}4d_{5/2})_2 4f_{5/2}$	7/2	104.44	9.2894(14)	7.9146(14)	7.8205(14)
$3d_{5/2}^{-1}(4f_{7/2}^2)_4$	9/2	175.05	7.7139(13)	8.1443(13)	8.3270(13)
$(3d_{5/2}^{-1}4f_{5/2})_2 4f_{7/2}$	7/2	190.52	8.1013(14)	8.2794(14)	8.3284(14)
$3d_{5/2}^{-1}(4f_{7/2}^2)_6$	9/2	191.38	3.2715(14)	3.2970(14)	3.3139(14)
$3d_{3/2}^{-1}(4f_{5/2}^2)_2$	7/2	252.17	1.4909(14)	1.6350(14)	1.7578(14)
$3d_{3/2}^{-1}(4f_{5/2}^2)_4$	7/2	264.91	5.1589(14)	5.1678(14)	5.2254(14)
$3d_{3/2}^{-1}(4f_{5/2}^2)_2$	3/2	279.25	6.7833(13)	6.8798(13)	7.1236(13)
$(3d_{5/2}^{-1}4f_{5/2})_1 4f_{7/2}$	5/2	287.87	7.6736(13)	7.7060(13)	7.9606(13)
$(3d_{5/2}^{-1}4p_{1/2})_2 5p_{3/2}$	1/2	324.74	5.0935(13)	6.8837(13)	6.4543(13)
$(3d_{3/2}^{-1}4s_{1/2})_2 5d_{3/2}$	1/2	393.96	1.1723(14)	1.3709(14)	1.2730(14)
$(3d_{5/2}^{-1}4p_{1/2})_3 5d_{5/2}$	1/2	428.41	1.0771(14)	1.2546(14)	1.2051(14)
$(3d_{3/2}^{-1}4p_{1/2})_1 5d_{3/2}$	1/2	505.24	1.0803(14)	1.2825(14)	1.1858(14)
$(3d_{5/2}^{-1}4p_{3/2})_3 5d_{5/2}$	3/2	574.02	8.5545(13)	1.0342(14)	9.7995(13)
$(3d_{5/2}^{-1}4d_{5/2})_0 5p_{1/2}$	1/2	615.95	6.5320(13)	5.7005(13)	5.7942(13)
$(3d_{3/2}^{-1}4p_{3/2})_3 5d_{3/2}$	3/2	647.44	9.8468(13)	9.6967(13)	9.5598(13)
$(3d_{3/2}^{-1}4d_{3/2})_0 5p_{1/2}$	1/2	702.96	3.2023(14)	1.2041(14)	1.0146(14)
$(3d_{5/2}^{-1}4d_{5/2})_1 5d_{3/2}$	3/2	737.11	9.7113(13)	1.1538(14)	9.5433(13)
$(3d_{5/2}^{-1}4d_{5/2})_0 5d_{3/2}$	3/2	763.57	9.8629(13)	1.3553(14)	1.3748(14)
$(3d_{3/2}^{-1}4d_{3/2})_0 5p_{3/2}$	3/2	768.55	3.8933(14)	3.0014(14)	3.0776(14)
$(3d_{5/2}^{-1}4d_{5/2})_3 5d_{5/2}$	5/2	768.88	9.9533(13)	1.0685(14)	7.5816(13)
$(3d_{5/2}^{-1}4d_{5/2})_0 5d_{5/2}$	5/2	777.99	7.3250(13)	7.1309(13)	7.3601(13)
$(3d_{3/2}^{-1}4d_{3/2})_3 5d_{3/2}$	3/2	811.64	4.4063(13)	5.5327(13)	6.2072(13)
$(3d_{3/2}^{-1}4d_{3/2})_2 5d_{3/2}$	3/2	814.56	7.0037(13)	1.1633(14)	1.0004(14)
$(3d_{5/2}^{-1}4d_{3/2})_3 5f_{7/2}$	5/2	818.02	1.0097(14)	1.0031(14)	8.2268(13)
$(3d_{3/2}^{-1}4d_{5/2})_3 5d_{3/2}$	5/2	843.76	1.1382(14)	1.2378(14)	1.1687(14)
$(3d_{3/2}^{-1}4d_{3/2})_0 5d_{3/2}$	3/2	846.90	2.5559(14)	2.5612(14)	2.6833(14)
$(3d_{5/2}^{-1}4d_{5/2})_2 5f_{7/2}$	7/2	849.45	9.2981(13)	9.3225(13)	9.1084(13)
$(3d_{5/2}^{-1}4d_{5/2})_0 5f_{5/2}$	5/2	856.79	6.3630(13)	5.8296(13)	6.0097(13)
$(3d_{3/2}^{-1}4d_{3/2})_0 5d_{5/2}$	5/2	862.33	3.4915(14)	1.9267(14)	2.0729(14)
$(3d_{3/2}^{-1}4f_{7/2})_2 5p_{1/2}$	5/2	864.53	3.3853(13)	6.3485(13)	6.2707(13)
$(3d_{3/2}^{-1}4f_{5/2})_1 5p_{1/2}$	1/2	884.30	4.1461(13)	1.2125(14)	1.3807(14)
$(3d_{3/2}^{-1}4d_{3/2})_3 5f_{5/2}$	5/2	897.64	5.2337(13)	5.5362(13)	5.4864(13)
$(3d_{3/2}^{-1}4d_{3/2})_2 5f_{5/2}$	5/2	903.42	6.2938(13)	6.2800(13)	5.9371(13)

TABLE I. (*Continued.*)

Conf.	J	ΔE (eV)	A^a (s^{-1})		
			A	B	C
$(3d_{3/2}^{-1}4d_{3/2})_0 5f_{7/2}$	7/2	946.36	9.0914(13)	1.0794(14)	9.7210(13)
$(3d_{5/2}^{-1}4f_{7/2})_3 5d_{3/2}$	5/2	946.96	3.4635(14)	2.7019(14)	2.6656(14)
$(3d_{5/2}^{-1}4d_{7/2})_5 5d_{5/2}$	7/2	951.85	2.7128(14)	1.3206(14)	1.2547(14)
$(3d_{3/2}^{-1}4f_{7/2})_4 5d_{3/2}$	7/2	1028.30	7.8475(13)	1.0232(14)	9.4021(13)
$(3d_{5/2}^{-1}4f_{7/2})_3 5f_{7/2}$	9/2	1034.71	9.8710(13)	1.0354(14)	9.3044(13)
$(3d_{5/2}^{-1}4f_{7/2})_1 5f_{5/2}$	7/2	1039.92	4.9410(14)	5.0109(14)	5.1201(14)
$(3d_{5/2}^{-1}4f_{7/2})_1 5f_{7/2}$	9/2	1042.94	1.2390(14)	1.2381(14)	1.3531(14)
$(3d_{3/2}^{-1}4f_{5/2})_1 5d_{5/2}$	7/2	1047.85	1.4348(14)	1.1241(14)	1.4605(14)
$(3d_{3/2}^{-1}4f_{5/2})_4 5f_{5/2}$	7/2	1104.62	1.0224(14)	1.0447(14)	9.4677(13)
$(3d_{3/2}^{-1}4f_{5/2})_1 5f_{5/2}$	7/2	1126.43	2.1766(14)	2.1523(14)	2.2826(14)
$(3d_{3/2}^{-1}4f_{5/2})_1 5f_{7/2}$	9/2	1132.32	5.8792(14)	4.9187(14)	4.1183(14)
$(3d_{3/2}^{-1}4f_{5/2})_1 5g_{7/2}$	9/2	1173.72	1.8053(14)	1.6050(14)	1.6157(14)
$(3d_{3/2}^{-1}4f_{5/2})_1 5g_{9/2}$	11/2	1183.52	2.3429(14)	1.7765(14)	1.7663(14)

other. Figure 2 shows the total DR rate coefficients through $3d^9 4l4l'$ and $3d^9 4l5l'$ from different theoretical calculations. The diamonds represent the results of Yi *et al.* [26] by using a configuration averaged approach based on Cowan's quasirelativistic multiconfiguration Hartree-Fock-Relativistic code and distorted wave approximation. The other three theoretical results are obtained by level-by-level calculations. From the inspection of Fig. 2, one can see that the results from level-by-level calculations agree very well with each other. Yet Yi *et al.* [26] predicted larger values at low temperature. The DR rate coefficients at low temperature are mainly contributed by the levels of $3d^9 4d4f$. For levels belonging to this configuration, some are located below and some above the IP ($E_I = 2942.79$ eV) of Au^{50+}, which can be easily seen from Fig. 3. In the level-by-level calculations, the levels below the IP do not contribute to the autoionization rate. Yi *et al.* [26] adopted a configuration averaged approach, where the nonautoionization levels of $3d^9 4d4f$ are included in the calculation and thus a larger rate coefficient is obtained by Yi *et al.* [26]. By adding the configurations included in the calculations step by step, we estimated the accuracy of the level-by-level autoionization and DC rates should be better

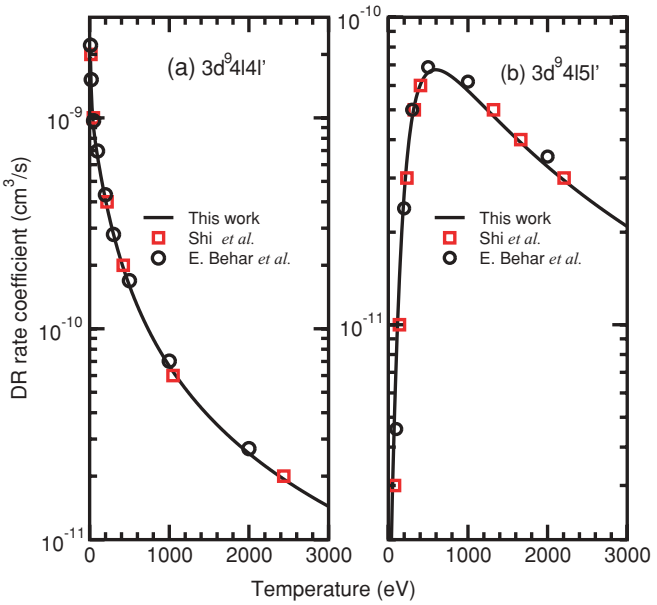

FIG. 1. (Color online) DR rate coefficient of Au^{50+} through the configurations of (a) $3d^9 4l4l'$ and (b) $3d^9 4l5l'$, respectively. The solid line, circles, and squares represent the results of this work, Behar *et al.* [27], and Shi *et al.* [24], respectively.

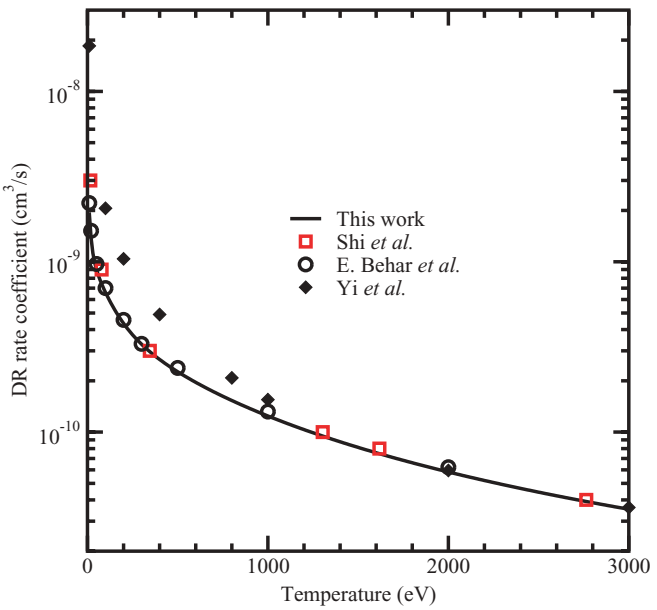

FIG. 2. (Color online) DR rate coefficient of Au^{50+} through $3d^9 4l4l'$ and $3d^9 4l5l'$. The solid line, circles, squares, and diamonds represent the results of this work, Behar *et al.* [27], Shi *et al.* [24], and Yi *et al.* [26], respectively.

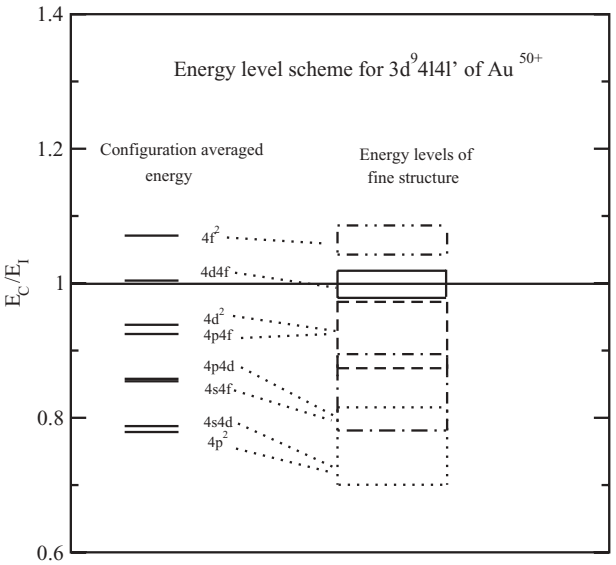

FIG. 3. Energy of the doubly excited configurations E_C with the $3d^9 4l 4l'$ complex relative to ionization potential ($E_I = 2942.79$ eV) of Au^{50+}. The energies are indicated by a finite vertical range representing the full level spread within each configuration.

than 20% for the strong ones. In fact, the relative difference between our results and those of Behar *et al.* [27] is less than 10% for the DR rate coefficients of Au^{51+} in the ground state through $3d^9 4l 4l'$ and $3d^9 4l 5l'$ of Au^{50+}.

Accurate level-by-level autoionization rates can be transformed to configuration-by-configuration ones according to statistical averaging

$$A^a_{CC'} = \frac{\sum_{i\in C}\sum_{j\in C'} g_i A^a_{ij}}{\sum_{i\in C} g_i}, \tag{6}$$

where $A^a_{CC'}$ represents the autoionization rate from configuration C to C', i and j represent the fine-structure levels belonging to the configurations C and C', respectively, and g_i is the statistical weight of the level i. Table II lists the configuration-by-configuration autoionization rates from the doubly excited configurations $3d^9 4lnp$ and $3d^9 4lnf$ ($n = 4,5,6,\ldots,9$) of Au^{50+} to the ground configuration $3d^{10}$ of Au^{51+}. To have a quantitative understanding of the CI effects, we gave the corresponding results obtained by single configuration (SC) calculations which are listed in the third column of Table II.

According to our estimate of the accuracy of level-by-level calculations, we evaluate that the configuration-by-configuration autoionization and DC rates obtained by large-scale CI calculations should be accurate to be 30%. For the strong ones, the accuracy should be even higher. Behar *et al.* [27] compared their DR rate coefficients obtained by the level-by-level calculations with those of a configuration averaging method [28] for the $3d^9 4f 5f$ configuration at temperature of 1 keV and it was found that the configuration averaging method overestimated the configuration-by-configuration DR rate by 58%. In the configuration averaging method, some extra autoionization and radiative decay channels were omitted in the configuration-average DR rates. As pointed out by Behar *et al.* [27], such an overestimation should be attributed to the poor correlation between the autoionization and radiative decay coefficients for individual levels. However, all these physical effects were adequately considered in our detailed level-by-level calculations and those of Behar *et al.* [27]. Therefore, the accuracy of the configuration averaging method [28] is lower than our DR rates and those of Behar *et al.* [27] obtained by the detailed level-by-level calculations. Thus our estimation of accuracy of 30% for the autoionization and DC rates obtained by large-scale CI calculations is reasonable.

The configuration-by-configuration autoionization rate given in Table II obtained by large-scale CI calculations can be used to check the accuracy of rate coefficients obtained by the analytical formula in various CR models. One of the widely used analytical formulas can be found in Chung *et al.* [20] and Florido *et al.* [21], who applied an approximate mean value for the electron capture rate by integrating the hydrogenic cross section of electron impact excitation [29,30] and then obtained the autoionization rate according to the principle of detailed balance. Taking the autoionization of the $3d^9 4lnp$ configuration as an example to describe the procedure, the autoionization rate can be obtained by applying two steps: the configuration $3d^9 4lnp$ autoionizes to an auxiliary one $3d^9 np$ and then decays to the steady configuration $3d^{10}$. The process of the calculation can be described as

$$3d^9 4lnp \rightarrow 3d^9 np + e^-, \tag{7}$$

and then

$$3d^9 np \rightarrow 3d^{10} + h\nu. \tag{8}$$

The autoionization rate reads as

$$A^a_{CC'} = \frac{32 m_e a_0^3 I_H^3}{\sqrt{3}\hbar^3} \frac{g_{C'} Z^2_{eff} f_{C'M}}{g_C n^3 E_{CC'}} g(u), \tag{9}$$

where $f_{C'M}$ is the oscillator strength of the transition between the auxiliary configuration $M(3d^9 np)$ and the steady configuration $C'(3d^{10})$ of the recombined ion, $E_{CC'}$ is the energy difference between the autoionized and recombined ion, $g(u)$ is the effective Gaunt factor [21], a_0 is the Bohr radius, I_H is the Rydberg constant, and Z_{eff} is the effective charge of autoionized ions.

From the inspection of Table II, one can find that the CI effect is complex and it behaves differently for different Rydberg series. Among all the given Rydberg series, CI has the weakest effect on $3d^9 4fnf$ ($n = 4,5,6,\ldots,9$) series. For this series, the relative difference between autoionization rates obtained by CI and SC is within 17% (for $3d^9 4f 5f$). However, for any other Rydberg series, the CI effect can greatly enhance or reduce the rates and the relative difference can exceed 100%. For example, the autoionization rate of $3d^9 4s6f$ obtained by CI calculation is nearly six times larger than the corresponding result by SC calculation. However, for $3d^9 4d5f$, the CI result is only a half of the SC calculation. For the same Rydberg series, the trend with CI can also be greatly different. Take $3d^9 4snf$ as an example. The CI effect can enhance the autoionization rate by a factor of 6 for $3d^9 4s6f$, while it increases by 14%, 7%, 80%, and 60% for $3d^9 4snf$ ($n = 5,7,8,9$), respectively. A similar conclusion can be applied for the $3d^9 4pnf$ Rydberg series.

TABLE II. Configuration-configuration autoionization rates from configurations $3d^9 4lnf$ and $3d^9 4lnp$ of Au^{50+} to the ground configuration of Au^{51+}. The labels have the same meaning as those in Table I.

Conf.	CI	$A^a_{CC'}$ (s^{-1}) SC	Formula (9)	ΔE (eV)	Ratios
$3d^9 4s5f$	1.2495(12)	1.1028(12)	2.2977(14)	419.94	183.89
$3d^9 4s6f$	3.2325(12)	4.6999(11)	4.4044(13)	876.67	13.63
$3d^9 4s7f$	2.7168(11)	2.5454(11)	1.7157(13)	1150.19	63.15
$3d^9 4s8f$	2.8031(11)	1.5622(11)	8.7440(12)	1326.76	31.19
$3d^9 4s9f$	1.6719(11)	1.0377(11)	3.4047(12)	1447.28	20.36
$3d^9 4p5f$	3.6663(11)	3.6569(11)	5.1251(13)	627.57	139.79
$3d^9 4p6f$	4.9217(11)	1.8934(11)	1.1868(13)	1084.47	24.11
$3d^9 4p7f$	2.5577(11)	1.1617(11)	4.8436(12)	1358.07	18.94
$3d^9 4p8f$	4.8346(11)	7.7008(10)	2.5198(12)	1534.67	5.21
$3d^9 4p9f$	4.3901(10)	5.3718(10)	9.9234(11)	1655.21	22.60
$3d^9 4d4f$	2.5785(13)	3.1867(13)	6.8283(15)	11.88	264.81
$3d^9 4d5f$	3.3303(12)	6.6701(12)	2.2403(13)	861.41	6.73
$3d^9 4d6f$	3.0429(12)	3.5283(12)	5.8582(12)	1318.24	1.93
$3d^9 4d7f$	1.6239(12)	2.1354(12)	2.4794(12)	1591.79	1.53
$3d^9 4d8f$	1.4153(12)	1.3847(12)	1.3121(12)	1768.37	0.93
$3d^9 4d9f$	8.2827(11)	9.5130(11)	5.2174(11)	1888.89	0.63
$3d^9 4f^2$	3.5532(13)	3.4882(13)	5.9776(14)	208.77	16.82
$3d^9 4f5f$	9.5256(12)	1.1160(13)	1.3077(13)	1054.04	1.37
$3d^9 4f6f$	4.8967(12)	5.4892(12)	3.6524(12)	1510.28	0.75
$3d^9 4f7f$	2.7245(12)	3.1526(12)	1.5806(12)	1783.56	0.58
$3d^9 4f8f$	1.7770(12)	1.9965(12)	8.4557(11)	1960.00	0.48
$3d^9 4f9f$	1.2419(12)	1.3504(12)	3.3836(11)	2080.45	0.27
$3d^9 4s5p$	8.8757(11)	2.8485(11)	4.3427(13)	219.51	48.93
$3d^9 4s6p$	2.1683(11)	1.1742(11)	4.4710(12)	766.35	20.62
$3d^9 4s7p$	2.8253(11)	6.1203(10)	1.5470(12)	1082.85	5.48
$3d^9 4s8p$	6.3139(10)	3.6428(10)	7.4982(11)	1282.60	11.88
$3d^9 4s9p$	9.0372(10)	2.3653(10)	2.8612(11)	1416.75	3.17
$3d^9 4p5p$	1.9280(12)	6.7861(11)	7.4409(12)	427.05	3.86
$3d^9 4p6p$	4.2617(11)	2.9774(11)	1.1724(12)	974.14	2.75
$3d^9 4p7p$	2.6244(11)	1.6226(11)	4.3263(11)	1290.72	1.65
$3d^9 4p8p$	2.9296(11)	9.9537(10)	2.1508(11)	1490.51	0.73
$3d^9 4p9p$	3.2447(11)	6.5858(10)	8.3167(10)	1624.68	0.26
$3d^9 4d5p$	3.9509(12)	4.8513(12)	2.8828(12)	661.35	0.73
$3d^9 4d6p$	1.8853(12)	2.5854(12)	5.6725(11)	1208.05	0.30
$3d^9 4d7p$	8.2628(11)	1.5457(12)	2.1977(11)	1524.52	0.27
$3d^9 4d8p$	9.7177(11)	1.0105(12)	1.1155(11)	1724.25	0.11
$3d^9 4d9p$	6.2575(11)	6.9149(11)	4.3625(10)	1858.39	0.70
$3d^9 4f5p$	1.8007(12)	6.2212(11)	1.5949(12)	853.87	0.89
$3d^9 4f6p$	4.8781(11)	3.4569(11)	3.4964(11)	1399.95	0.72
$3d^9 4f7p$	2.7061(11)	2.1688(11)	1.3944(11)	1716.19	0.52
$3d^9 4f8p$	1.3354(11)	1.4255(11)	7.1713(10)	1915.81	0.54
$3d^9 4f9p$	1.0883(11)	9.8709(10)	2.8249(10)	2049.89	0.26

It can be seen from Table II that the autoionization rates from configuration $3d^9 4lnl'$ ($n = 6,7$ or even higher) are comparable to those from $3d^9 4l5l'$. As a result, the higher n shells will have an evident contribution to the DR rate coefficient. Figure 4 shows partial DR rates through configurations $3d^9 4lnl'$ ($n = 4$–9) and their sum as a function of electron temperature. From the inspection of Fig. 4, one can see that the contribution of the higher n shells increases with the increase of electron temperature. At 1 keV, the contributions to the sum of DR rates are 40.1%, 34.7%, 13.1%, 6.0%, 3.7%, and 2.4%, respectively, for the $3d^9 4lnl'$ ($n = 4$–9). The $n = 6$–9 shells contribute to the sum by 25%. When the temperature increases to 3 keV, they are 24.2%, 35.1%, 18.2%, 10.2%, 7.2%, and 5.1%, respectively, for the $3d^9 4lnl'$ ($n = 4$–9). The $n = 6$–9 shells contribute to the sum by 40.7%. Obviously, it is not enough for the total DR rates by including contributions up to $n = 9$. The contributions from $n > 9$ can be estimated by extrapolation [25,31], applying an n^{-3} scaling, which amounts to 9.7% and 20.5%, respectively, to the total DR rates at temperatures of 1 and 3 keV.

The autoionization rates obtained by the analytical formula [Eq. (9)] are also given in Table II. The last column gives

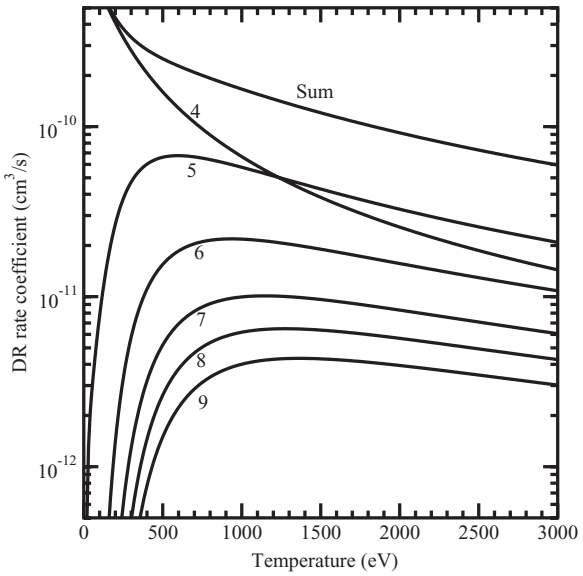

FIG. 4. Partial DR rate coefficients through configurations of $3d^9 4lnl'$ ($n = 4$–9) and their sum as a function of electron temperature. The labels 4–9 represent the value of n.

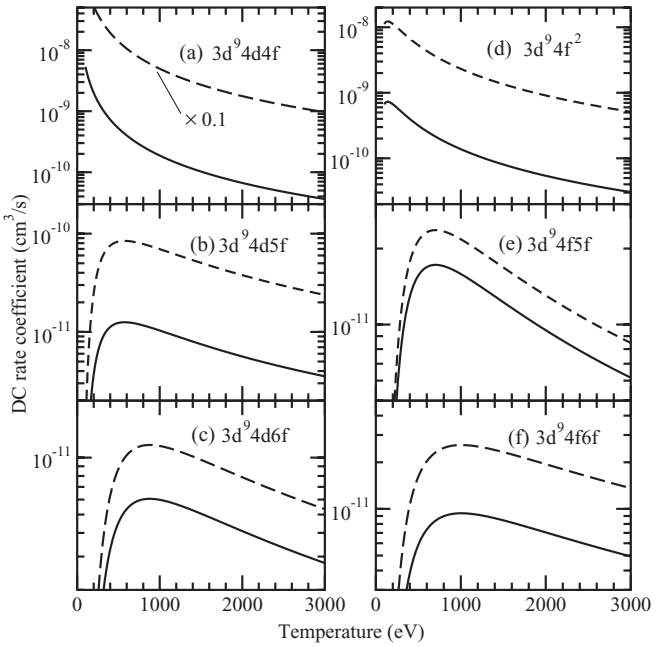

FIG. 5. The rate coefficients of DC from $3d^{10}$ to $3d^9 4dnf$ and $3d^9 4fnf$ ($n = 4,5,6$) as a function of temperature. The solid line shows the results obtained by the large-scale CI calculation and the dashed line the results of the analytical formula.

the ratio of autoionization rates calculated by the analytical formula and by large-scale CI level-by-level calculations. As shown previously, the results of the CI calculations agree very well for different independent work, and therefore our CI results should be reliable. The ratio between the autoionization rates of the analytical formula and CI calculations reflects the validity of the analytical formula. From the inspection of Table II, one can find that the analytical formula predicted much larger autoionization rates for the Rydberg series of $3d^9 4snf$, $3d^9 4pnf$, and $3d^9 4snp$, while it also predicted much smaller values for the Rydberg series of $3d^9 4dnp$ and $3d^9 4fnp$. The largest discrepancy predicted by the analytical formula is more than two orders of magnitude larger (for $3d^9 4d4f$). While for configuration $3d^9 4d8p$, the analytical formula predicted the autoionization rates nearly one order of magnitude smaller than the CI result. The biggest discrepancies originate from configurations of $3d^9 4s5f$, $3d^9 4p5f$, and $3d^9 4d4f$ (ratio of 183.89, 139.79, and 264.81, respectively), whose energy are close to IP. For a given Rydberg series, the variational trend differs greatly with the increase of principle quantum number of the outmost valence electron. Take the $3d^9 4dnf$ series to illustrate this trend. The ratio expands from 264.81 ($3d^9 4s4f$) to 0.63 ($3d^9 4s9f$), which is successively smaller. With the increase of the principle quantum number of the outmost valence electron, the agreement gets better and better. Such a character of disproportion gives rise to a great challenge in using the analytical formula.

DC rate coefficients show a similar trend to the autoionization rates predicted by the analytical formula. As illustrative examples, Fig. 5 shows the DC rate coefficients from $3d^{10}$ of Au^{51+} to $3d^9 4dnf$ and $3d^9 4fnf$ ($n = 4,5,6$) of Au^{50+} as a function of temperature, where the solid line is the DC rates of large-scale CI calculations and the dashed line is the results of the analytical formula. In Fig. 5(a), the DC rate coefficient from $3d^9 4d4f$ obtained by the analytical formula is multiplied by a factor of 0.1 for more clear viewing. The autoionization and DC processes play an important role on the ionization balance for NLTE plasmas. There are dramatic discrepancies for different CR models with the inclusion of autoionization and DC processes and as a result, there are dramatic discrepancies between different NLTE models of population distribution kinetics. Accurate methods should be used to improve the accuracy of autoionization and rates to better model the NLTE plasmas.

IV. CONCLUSION

In conclusion, large-scale CI calculations with detailed level accounting were carried out for the autoionization rates of Au^{50+} and DC rates of Au^{51+}. The accuracy should be better than 20% for strong autoionized levels. Our results of DR process through $3d^9 4lnl'$ ($n = 4,5$) agree excellently with other theoretical results reported in the literature. The relative difference between our results and those of Behar *et al.* [27] is less than 10% for the DR rate coefficients of Au^{50+} in the ground state through $3d^9 4l4l'$ and $3d^9 4l5l'$ of Au^{51+}. In the modeling of NLTE plasmas, a detailed configuration accounting method is the usual choice. Therefore, we transformed the level-by-level autoionization and DC rates to configuration-by-configuration ones, which should be accurate to be 30%. These rate coefficients were used to check the validity of the analytical formula in CR models. The autoionization and DC rates predicted by the analytical formula can be more than two orders larger for configurations whose energy are close to IP, or nearly one order smaller than the large-scale CI calculations for configurations located far above IP. Accurate methods should be used to obtain autoionization and DC rates in NLTE plasma modeling.

ACKNOWLEDGMENTS

This work was supported by the National Natural Science Foundation of China under Grants No. 10774191, No. 10878024, and No. 10734140, and the National Basic Research Program of China (973 Program) under Grant No. 2007CB815105.

[1] R. W. Lee, J. K. Nash, and Yu. Ralchenko, J. Quant. Spectrosc. Radiat. Transfer **58**, 737 (1997).
[2] C. Bowen, A. Decoster, C. J. Fontes, K. B. Fournier, O. Peyrusse, and Yu. V. Ralchenko, J. Quant. Spectrosc. Radiat. Transfer **81**, 71 (2003).
[3] C. Bowen, R. W. Lee, and Yu. Ralchenko, J. Quant. Spectrosc. Radiat. Transfer **99**, 102 (2006).
[4] J. G. Rubiano, R. Flordo, C. Bowen, R. W. Lee, and Yu. Ralchenko, High Energy Density Phys. **3**, 225 (2007).
[5] C. J. Fontes, J. Abdallah, Jr., C. Bowen, R. W. Lee, and Yu. Ralchenko, High Energy Density Phys. **5**, 15 (2009).
[6] H.-K. Chung and R. W. Lee, High Energy Density Phys. **5**, 1 (2009).
[7] H. A. Scott and S. B. Hansen, High Energy Density Phys. **6**, 39 (2010).
[8] Z. Q. Wu, B. A. Zhang, and Y. B. Qiu, Chin. Phys. **9**, 519 (2000).
[9] J. R. Albritton and B. G. Wilson, Phys. Rev. Lett. **83**, 1594 (1999).
[10] Y. Hahn, Rep. Prog. Phys. **60**, 691 (1997).
[11] V. L. Jacobs, J. Quant. Spectrosc. Radiat. Transfer **54**, 195 (1995).
[12] R. Doron, E. Behar, P. Mandelbaum, and J. L. Schwob, J. Quant. Spectrosc. Radiat. Transfer **65**, 161 (2000).
[13] G. Faussurier, C. Blancard, and E. Berthier, Phys. Rev. E **63**, 026401 (2001).
[14] J. Bauche, C. Bauche-Arnoult, and O. Peyrusse, High Energy Density Phys. **5**, 51 (2009).
[15] V. L. Jacobs, High Energy Density Phys. **5**, 80 (2009).
[16] S. Mazevet and J. Abdallah, J. Phys. B **39**, 3419 (2006).
[17] C. J. Fontes, J. Colgan, H. L. Zhang, and J. Abdallah, J. Quant. Spectrosc. Radiat. Transfer **99**, 175 (2006).
[18] A. Bar-Shalom, M. Klapisch, and J. Oreg, J. Quant. Spectrosc. Radiat. Transfer **71**, 169 (2001).
[19] Y. V. Ralchenko and Y. Maron, J. Quant. Spectrosc. Radiat. Transfer **71**, 609 (2001).
[20] H.-K. Chung, M. H. Chen, W. L. Morgan, Y. Rachenko, and R. W. Lee, High Energy Density Phys. **1**, 3 (2005).
[21] R. Florido, R. Rodríguez, J. M. Gil, J. G. Rubiano, P. Martel, E. Mínguez, and R. C. Mancini, Phys. Rev. E **80**, 056402 (2009).
[22] M. F. Gu, Astrophys. J. **582**, 1241 (2003).
[23] R. D. Cowan, *The Theory of Atomic Structure and Spectra* (University of California Press, Berkeley, CA, 1981).
[24] X. H. Shi, C. Y. Chen, Y. S. Wang, and M. F. Gu, Chin. Phys. Lett. **21**, 1937 (2004).
[25] E. Behar, P. Mandelbaum, J. L. Schwob, A. Bar-Shalom, J. Oreg, and W. H. Goldstein, Phys. Rev. A **54**, 3070 (1996).
[26] Y. G. Yi, Z. J. Zheng, J. Yan, P. Li, Q. Y. Fang, and Y. B. Qiu, Acta Phys. Sin. **51**, 2740 (2002).
[27] E. Behar, P. Mandelbaum, J. L. Schwob, A. Bar-Shalom, J. Oreg, and W. H. Goldstein, Phys. Rev. A **52**, 3770 (1995).
[28] C. Bauche-Arnoult, J. Bauche, E. Luc-Koenig, J. F. Wyart, R. M. More, C. Chenais-Popovics, J. C. Gauthier, J. P. Geindre, and N. Tragin, Phys. Rev. A **39**, 1053 (1989).
[29] A. Burgess, Astrophys. J. **139**, 776 (1964).
[30] H. R. Griem, *Principles of Plasma Spectroscopy* (Cambridge University Press, Cambridge, England, 1997).
[31] Y. Hahn, Adv. At. Mol. Opt. Phys. **21**, 123 (1985).